PCCP

Theoretical Study of the Reaction Mechanism and Kinetics of the Phenyl + Propargyl Association

Journal:	*Physical Chemistry Chemical Physics*
Manuscript ID	CP-ART-01-2020-000306.R1
Article Type:	Paper
Date Submitted by the Author:	03-Mar-2020
Complete List of Authors:	Morozov, Alexander; Florida International University Mebel, Alexander; Florida International University, Chemistry and Biochemistry

Theoretical Study of the Reaction Mechanism and Kinetics of the Phenyl + Propargyl Association

Alexander N. Morozov and Alexander M. Mebel*

Department of Chemistry and Biochemistry, Florida International University, Miami, Florida 33199, USA

E-mail: mebela@fiu.edu.

ABSTRACT Potential energy surface for the phenyl + propargyl radical recombination reaction has been studied at the CCSD(T)-F12/cc-pVTZ-f12//B3LYP/6-311G** level of theory for the closed-shell singlet species and at the triplet-singlet gap CASPT2/cc-pVTZ-CCSD(T)-F12/cc-pVTZ-f12//CASSCF/cc-pVTZ level of theory for the diradical species. High-pressure limit rate constants for the barrierless channels were evaluated with variable reaction coordinate transition state theory (VRC-TST). Rice-Ramsperger-Kassel-Marcus Master Equation (RRKM-ME) calculations have been performed to assess temperature- and pressure–dependent phenomenological rate constants and product branching ratios. The entrance channels of the radical association reaction produce 3-phenyl-1-propyne and phenylallene which can further dissociate/isomerize into a variety of unimolecular and bimolecular products. Theoretical evidence is presented that, at combustion relevant conditions, the phenyl + propargyl recombination provides a feasible mechanism for the addition of a second five-member ring to the first six-member aromatic ring producing the prototype two-ring species indene and indenyl. Rate expressions for all important reaction channels in a broad range of temperatures and pressures have been generated for kinetic modeling.

1. INTRODUCTION

Understanding the mechanism of soot formation in flames of hydrocarbon fuels is an important research goal as carbonaceous particles released in incomplete combustion often exhibit hazardous health and environmental effects. Sampling studies of hydrocarbon flames[1] reveal that mass growth of soot particles is linked to ring expansion in polycyclic aromatic hydrocarbons (PAH) via recombination reactions of resonantly stabilized free radicals (RSFRs).[2] The key mechanisms of the formation of the "first ring" species, benzene (C_6H_6) or phenyl radical (C_6H_5), is well established.[3] A quantitatively accurate description of the formation of the prototype two-ring species indenyl (C_9H_7), indene (C_9H_8), and naphthalene ($C_{10}H_8$) by expansion of the "first ring" species is required for further understanding of the mechanism of PAH formation. Importantly, this second step is expected to provide a model of a recurring addition of one extra six- or five-member ring to form larger PAHs.[4] Both theory and experiment agree that the radical-radical recombination reactions of C_3 RSFRs, propargyl (C_3H_3) and allyl (C_3H_5), is an important route of the "first ring" growth to polycyclic species.[3,5] The role of propargyl and allyl in the formation of the two-ring PAHs is a subject of the ongoing theoretical research.[6,7] The fundamental character of such studies is supported by the available experimental observations. For example, Ruwe et al. carried out the experimental study of influence of the molecular structure of *n*-pentane, 1-pentene and 2-methyl-2-butene (2M2B) flames on the PAH growth.[8] They found that the abundance of indene and naphthalene in the alkene flames relative to the alkane flame, i. e. *n*-pentane < 1-pentene < 2M2B, can be traced back to the difference in the concentrations of the C_5 and C_3 RSFR precursors cyclopentadienyl (C_5H_5) and propargyl.[8] In their experiments, the alkene flames were also found to be rich, relative to the alkane flame, in the cyclic C_6 and C_7 species, i. e. *n*-pentane < 1-pentene < 2M2B. The observed correlation between the C_6, C_7, propargyl and two-ring PAH species indicates that the C_3 RSFRs are likely

to participate in the second ring formation along with the supposed by the authors C_5 RSFR chemistry. The same conclusion can be drawn from another detailed investigation of the PAH growth and soot formation in a variety of pure 1-alkene fuels by Wang et al.[9] It was found that, in addition to benzene formation, propargyl and cyclopentadienyl are also likely precursors of larger PAHs. A quantitatively accurate characterization of the PAH growth pathways requires predictive calculations of temperature (T) and pressure (p) dependent rate constants for the reactions involving C_3 RSFRs leading to the formation of an extra aromatic ring. In the absence of direct experimental data, high-level ab initio calculations of potential energy surfaces (PESs) combined with the state-of-the-art methods of Variable Reaction Coordinate-Transition State Theory (VRC-TST) together with the master equation approach provide a theoretical framework within which the *T, p*-dependent rate constants of interest can be evaluated with "kinetic accuracy".[5,10]

Here we present a theoretical study of the association reaction of the phenyl radical (C_6H_5) with the C_3 radical propargyl, a possible source of the prototype two-ring species indenyl and indene. As a part of the broader project to unravel the mechanism of PAH expansion from one to two rings,[4] the present study is a follow-up to the study of the C_3 RSFR allyl (C_3H_5) association reaction with the phenyl radical.[7] In the recombination reaction of phenyl and allyl radicals, the route to 1-phenylallyl, a ready C_9H_9 precursor of indene, requires H removal from the C_9H_{10} intermediate, 3-phenylpropene: $C_6H_5 + C_3H_5 \rightarrow C_6H_5CH_2CHCH_2 \rightarrow C_6H_5CHCHCH_2 + H$. The kinetics calculations of the phenyl + allyl reaction showed that, at combustion relevant conditions, the benzyl ($C_6H_5CH_2$) + vinyl (C_2H_3) bimolecular product is favored over 1-phenylallyl + H due to the preferable dissociation entropy.[7] Also, because of collisional stabilization, the 3-phenylpropene adduct itself is the major product of the phenyl + allyl

reaction.[7] Similar to the phenyl + propene reaction,[11] 3-phenylpropene can undergo secondary H-abstraction by available radicals to produce the indene precursor 1-phenylallyl.

The phenyl + propargyl reaction begins with barrierless association steps producing the closed-shell C_9H_8 species 3-phenyl-1-propyne or phenylallene (C_9H_8), reactions R1 and R2 respectively:

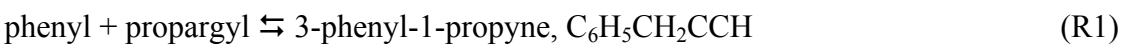

phenyl + propargyl ⇆ 3-phenyl-1-propyne, $C_6H_5CH_2CCH$ (R1)

phenyl + propargyl ⇆ phenylallene, $C_6H_5CHCCH_2$ (R2)

Next, the C_9H_8 isomers may undergo entropy-driven H eliminations:

3-phenyl-1-propyne → C_6H_5CHCCH + H (R3)

phenylallene → C_6H_5CHCCH + H (R4)

phenylallene → $C_6H_5CCCH_2$ + H (R5)

Alternatively, 3-phenyl-1-propyne and phenylallene may undergo ring closure to form an enantiomeric mixture of the two-ring C_9H_8 intermediate:

phenylallene → $C_6H_5C_3H_3$-e1, (R6)

3-phenyl-1-propyne → $C_6H_5C_3H_3$-e1/e2, (R7)

The two-ring $C_6H_5C_3H_3$ intermediate may either dissociate yielding the indenyl + H bimolecular product:

$C_6H_5C_3H_3$-e1/e2 → $C_6H_4C_3H_3$, indenyl+ H, (R8)

or undergo H-shift and collisional stabilization yielding indene:

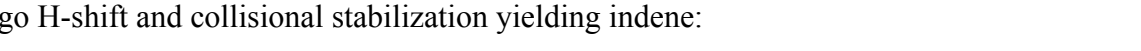

$C_6H_5C_3H_3$-e1/e2 → $C_6H_4C_3H_4$, indene (R9)

Finally, H elimination from indene to the indenyl + H bimolecular product proceeding without an exit barrier may also occur

indene → indenyl + H (R10)

In the present work, we carefully analyze all pathways of the reaction and generate rate constants for various reaction channels and predict the reaction outcome under different temperatures and pressures. These results should prove useful in kinetic modeling of PAH formation and growth in hydrocarbon flames.

2. THEORETICAL METHODS

Single-point energies of optimized local minima and transitions states with a closed-shell singlet character on the C_9H_8 PES relevant to the C_6H_5 + C_3H_3 reaction as well as of radical reactants and products were calculated using the explicitly correlated coupled clusters CCSD(T)-F12/cc-pVTZ-f12 method,[12-14] whereas their geometries were optimized and vibrational frequencies and zero-point energies (ZPE) were computed at the density functional theory (DFT) B3LYP/6-311G(d,p)[15-17] level. Alternatively, when T1 diagnostics of the stationary structures exceeded 0.02 indicating a diradical character of the wave function, the composite triplet-singlet gap method[6,18] was employed to calculate the energy at the CASPT2(12e,12o)[19,20]/cc-pVTZ[12]-CCSD(T)-F12/cc-pVTZ-f12 level of theory using the CASSCF(12e,12o)[21] method for the geometry optimization, vibrational frequencies, and ZPE calculations:

$$E = E_T[\text{CCSD(T)-F12/cc-pVTZ-f12}]+\Delta E_{S-T}[\text{CASPT2/cc-pVTZ}]+\text{ZPE}[\text{CASSCF/cc-pVTZ}] \quad (1)$$

where E_T denotes the energy of the triplet state calculated with CCSD(T)-F12, ΔE_{S-T} denotes the energy difference between singlet and triplet states calculated with CASPT2. Energies of diradical transition states were calculated relative to the corresponding local minima at the CASPT2(12e,12o)/cc-pVTZ level using CASSCF(12e,12o) for the geometry and frequency calculations. The (12e,12o) active space in the CASSCF and CASPT2 calculations included all π electrons and σ electrons involved in bond cleavage/formation or unpaired and the corresponding bonding and antibonding orbitals. All calculated local minima have no imaginary frequencies and transition states have one imaginary frequency. All reaction pathways were verified by carrying out intrinsic reaction coordinate (IRC)[22] calculations at the B3LYP/6-311G(d,p) level of theory. For diradical transition states, the IRC calculations were also performed at the CASSCF(12e,12o)/cc-pVDZ level of theory. The DFT calculations were carried out using the

Gaussian 09[23] program package, whereas the coupled clusters, CASSCF, and CASPT2 calculations were performed using the MOLPRO 2010[24] program.

The calculated PES and molecular properties were further used in statistical computations of the rate constants and product branching ratios. Energy and angular momentum-resolved (*E,J*-resolved) rate constants were computed using Rice-Ramsperger-Kassel-Marcus (RRKM) theory.[25] For the reactions with barriers, the rigid-rotor-harmonic-oscillator (RRHO) model was employed in the computation of the number of states of the transition states and of the density of states of the related local minima. Eckart's tunneling correction[26] was applied in the transition state calculations. Internal rotors were treated within the hindered-rotor approximation for the partition function, where the internal rotation potential were mapped out at the B3LYP/6-311G(d,p) level. *E,J*-resolved rate constants of the barierrless association and reverse dissociation reactions (R1-R5, R8, R10) were computed using variable reaction coordinate-transition state theory (VRC-TST).[5,27,28] Within this theory, a transition state is found by optimizing the reactive flux through a dividing surface between the reacting fragments and by optimizing the dividing surface itself. A multifaceted spherical dividing surface,[5] used in our calculations, is built as the equidistant surface between the pivot points assigned to the associating/dissociating fragments. At short-range distances between the active centers of the fragments (less than 5 Å), a pivot point represents the corresponding active orbital. Alternatively, centers of mass of the fragments serve as the pivot points at long-range distances.[5] The short-range pivot points used in the variational optimization of the flux through the dividing surface in reactions R1-R5, R8, and R10 are shown in Figure 1. For the phenyl radical the short-range pivot point was placed in the molecular plane along the radical orbital of the carbon lacking a C-H bond. In all reactions of interest involving phenyl, the optimal position of this pivot point was found at 1.25 bohr apart from the active carbon of phenyl. For the species with a π-radical, the pivot points were placed perpendicularly to the molecular plane and along the radical orbitals of the corresponding active carbons. Namely, for both CH and CH_2 terminals of propargyl in the phenyl + propargyl addition/dissociation, reactions R1 and R2, the optimal positions of the pivot points were found at 0.5 bohr apart from the active carbon of propargyl. In all H elimination reactions of interest the position of the H pivot point coincides with the H atom itself while the optimal position of C pivot points were found as follows: R3 at 1 bohr, R4 at 1.25 bohr, R5 at 0.25 bohr, R8 at 1 bohr, and R10 at 1 bohr away from the carbon atom. Note that due to the

computational limits related to the active space size (vide infra), variational optimization of the reactive flux in reaction R5 was carried out using a model system:

$$CH_2CCHCH_2CHCCH_2 \rightarrow CH_2CCHCH_2CCCH_2 + H \quad \text{(R11)}$$

The evaluation of the reactive flux through a dividing surface involves single-point calculations of the energy of the fragment-fragment complexes which are randomly generated on the dividing surface using optimized geometries of these fragments computed at the CASSCF(12e,12o)/cc-pVDZ level of theory when they are infinitely separated. Further, we use the term "rigid" referring to such a structure to denote the lack of their geometry relaxation. Single-point energies of "rigid" radical-radical structures were evaluated at the CASPT2(12e,12o)/cc-pVDZ[12] level of theory. To avoid discontinuities in the interaction potential of the radical fragments involving RSFRs like propargyl or allyl, the CASPT2 active space typically includes not only the delocalized radical and the orbital of the incipient bond but also the complete π system.[5,7] The (12e,12o) active space employed for both entrance channels of the propargyl + phenyl association, reactions R1 and R2, included relevant π and σ electrons of propargyl, (4e,4o), the π system of phenyl, (6e,6o), and the orbital of the incipient C-C bond, (2e,2o). For H eliminations from the C_9H_8 species in reactions R3, R4, R8, and R10 the chosen (10e,10o) active space included the π system of the corresponding C_9H_7 radical, (9e,9o), and the orbital of the H atom (1e,1o). H elimination from phenylallene in reactions R5 turned out to be a special case where the described above (10e,10o) active space as well as a larger (12e,12o) active space cannot produce a smooth interacting potential, which indicates that additional valence orbitals of the interacting fragments have to be included. VRC-TST CASPT2 calculations with an active space size large than (12e,12o) is beyond the resources available. To circumvent this problem, reaction R5 was simulated by reaction R11, i.e. the cyclical C_6H_5 part of phenylallene was replaced with a smaller CH_2CCHCH_2 analog that closely resembles the steric and chemical environment of the active carbon in reaction R5. The (10e,10o) active space employed in the energy calculations in the model system included the π system and relevant σ electrons of the corresponding C_7H_7 radical, (9e,9o), and the orbital of the H atom (1e,1o). In this case the calculations produced a smooth interaction potential. Single-point energies of the "rigid" radical-radical structures were further amended with a one-dimensional geometry relaxation correction[5] and a complete basis set (CBS) correction.[29] The one-dimensional geometry relaxation correction was calculated using

the CASSCF(12e,12o)/cc-pVDZ method to relax the "rigid" structures along the minimal energy path (MEP). The CBS correction was calculated using the CASPT2(12e,12o)/cc-pV*n*Z (*n* = D, T, Q) energies of the "rigid" MEP structures. To summarize, in the VRC-TST flux calculations the energies of the "rigid" structures sampled on the dividing surface were first probed at the CASPT2(12e,12o)/cc-pVDZ level of theory followed by the *ad hoc* one-dimensional relaxation and CBS corrections:

$$E = E_{rigid}[CASPT2/cc\text{-}pVDZ] + \Delta E[geom] + \Delta E[CBS] \quad (2),$$

where E_{rigid} is the single point energy of the interacting "rigid" fragments, $\Delta E[geom]$ is the geometry relaxation correction computed as the difference of CASPT2(12e,12o)/cc-pVDZ energy of the CASSCF(12e,12o)/cc-pVDZ optimized MEP structure corresponding to a particular value of the R_{CC}/R_{CH} distance and the "rigid" structure at the same R. Effects of geometry relaxation, $\Delta E[geom]$, are particularly important in the reactions of resonance-stabilized radicals due to their reduced attractiveness resulting in shorter separations for the transition state, and consequently large geometry relaxation energies along the minimal energy reaction path.[5] $\Delta E[CBS]$ was calculated as follows:

$$\Delta E[CBS] = \Delta E[pVQZ] + 0.69377\times(\Delta E[pVQZ] - \Delta E[pVTZ]), \quad (3)$$

where $\Delta E[pVTZ] = E_{rigid}[CASPT2/cc\text{-}VTZ] - E_{rigid}[CASPT2/cc\text{-}VDZ]$,

and $\Delta E[pVQZ] = E_{rigid}[CASPT2/cc\text{-}VQZ] - E_{rigid}[CASPT2/cc\text{-}VTZ]$.

T, p-dependences of the phenomenological rate constants were computed using the one-dimensional master equation[30] (ME) approach as implemented in the MESS software package.[31] Lennard-Jones and the collisional energy transfer parameters in ME calculations were taken from the previous study of the C_9H_x/Ar systems.[4] Namely, (ε/cm^{-1}, $\sigma/Å$) = (390, 4.46) were the Lennard-Jones parameters and n = 0.62, α_{300} = 424 cm^{-1} were used in the "exponential down" model[32] of the collisional energy transfer for the temperature dependence of the range parameter α for the deactivating wing of the energy transfer function $\alpha(T) = \alpha_{300}(T/300\ K)^n$. Cartesian coordinates, vibrational frequencies, relative energies, and hindered rotor potentials in the form of an input file for RRKM-ME calculations using the MESS code are provided in Electronic

Supplementary Information (ESI). ESI also contains modified Arrhenius expressions, which fit the calculated *T, p*-dependent rate constants (Table S1).

3. RESULTS AND DISCUSSION

Potential Energy Surface

The computed C_9H_8 PES of the phenyl + propargyl reaction is shown in Figure 2. The barrierless addition of propargyl to the radical site of phenyl by the CH_2 terminal, reaction R1, produces 3-phenyl-1-propyne (**i1**). The computed energy of 3-phenyl-1-propyne is -91.0 kcal/mol (all energy values are given relative to the energy of the phenyl + propargyl reactants). Let us first consider pathways where the two-ring species are formed. H–shift from the sp3 carbon in 3-phenyl-1-propyne results in the second ring closure via one of the -28.9 kcal/mol barriers leading to the enantiomeric mixture of the closed-shell singlet species **i3-e1,e2** with the computed energy of -93.0 kcal/mol, reaction R7. T1 diagnostics of these transition states, 0.034, indicates a diradical character of the wave function. A comparison of the B3LYP/6-311G(d,p)- and CASSCF(12e,12o)-optimized geometries of the transition state **i2** → **i3-e1** is shown in Figure 3a. For this transition state the CCSD(T)-F12/cc-pVTZ-f12 single-point energy of the B3LYP/6-311G(d,p) structure is 2.7 kcal/mol higher than the single-point energy of the CASSCF(12e,12o)/cc-pVTZ structure calculated at the CASPT2(12e,12o)/cc-pVTZ level of theory. To verify the CASSCF transition state geometry of the **i2** → **i3-e1** barrier, which appears to be the kinetic bottleneck for the second ring formation in phenyl + propargyl reaction, and to check for a possible shift of the transition state along the reaction coordinate, we performed IRCMax[33-35] calculations in which single-point energies of the IRC structures along the potential energy curve were refined at the CASPT2 level. The calculations resulted in a shift of the barrier location by 0.01 Å and in an increase of the activation energy by 0.05 kcal/mol, both values being within the accuracy of the employed methods.

At typical combustion conditions, the intermediate species **i3-e1, e2** have a metastable character and are immediate precursors of the prototype two-ring species indene (**i4**), -125.5 kcal/mol, and of indenyl as a part of the indenyl + H bimolecular product (**b1**), -46.0 kcal/mol. Reaction R8, **i3-e1/e2** → **b1**, is a dissociation without an exit barrier while reaction R9, **i3-e1/e2**

→ **i4**, proceeds via a 9.6 kcal/mol barrier, with the transition state positioned 83.4 kcal/mol below the initial reactants. Alternatives to the cyclization of 3-phenyl-1-propyne described above are entropy-driven decompositions occurring without barriers in reverse direction into the following bimolecular products: phenyl + propargyl (**b0**, reverse to reaction R1); H loss from the sp3 carbon resulting in the C_6H_5CHCCH + H product (**b2**, reaction R3), -11.9 kcal/mol; and, unlikely, decomposition into the benzyl, $C_6H_5CH_2$ + ethynyl, CCH product (**b4**), 21.3 kcal/mol. Intramolecular abstraction of H from the phenyl ring the by the side chain of 3-phenyl-1-propyne via a barrier located at -4.9 kcal/mol yields the *o*-benzyne, C_6H_4 + allene, C_3H_4 product (**b5**), at -9.6 kcal/mol.

The barrierless addition of propargyl to the radical site of phenyl by the CH terminal, reaction R2, produces phenylallene (**i2**). The computed energy of the phenylallene adduct, -95.6 kcal/mol, is -4.6 kcal/mol lower than that of the alternative **i1** adduct. H shifts from the terminal carbon of phenylallene result either in the closure of the five-member ring via a barrier located at -31.2 kcal/mol, **i2** → **i3-e1**, or in the closure of the three-member ring via a barrier located at -29.6 kcal/mol, **i2** → **i5**. Unlike **i1**, the TSs for H shifts in **i2** have wave functions with T1 diagnostics below 0.02 indicating a closed-shell singlet character of these transition states. There is a possibility of **i5**, -73.7 kcal/mol, converting into **i3-e2** via **i6**, -25 kcal/mol. However, this route is unlikely due to both low entropies and high energies of the corresponding transition states (Figure 2), e. g. the energy of the transition state for the **i6** → **i3-e2** isomerization is at 14.9 kcal/mol, well above the initial reactants. Phenylallene can be converted into indene through the **i2** → **i7** → **i4** isomerization sequence. This pathway is initiated by H transfer from the phenyl ring via a barrier with TS at -25.4 kcal/mol to form intermediate $C_6H_4CHCHCH$ (**i7**), -35.6 kcal/mol. Coupled cluster calculations showed that both the **i2** → **i7** TS (T1 = 0.041), and the **i7** intermediate (T1 = 0.051) represent singlets with a strong open-shell character. The same is true for TS **i7** → **i4** for the isomerization of **i7** into indene, -23.9 kcal/mol (T1 = 0.046). The B3LYP/6-311G(d,p)- and CASSCF(12e,12o)-optimized structures of TS **i2** → **i7**, intermediate **i7**, and TS **i7** → **i4** are compared in Figs. 3b, 3c, and 3d, respectively. The CCSD(T)-F12/cc-pVTZ-f12 single-point energies of the B3LYP/6-311G(d,p) structures of TS **i2** → **i7** and TS **i7** → **i4** are 4.2 and 0.8 kcal/mol lower than the single-point energies of the respective CASSCF(12e,12o)/cc-pVTZ structures calculated at the CASPT2(12e,12o)/cc-pVTZ level of theory. The CCSD(T)-F12/cc-pVTZ-f12 energy of the B3LYP/6-311G(d,p) structure of

intermediate **i7** is 0.2 kcal/mol higher than the energy of the respective CASSCF(12e,12o)/cc-pVTZ structure calculated with the composite triplet-singlet gap method (1). The CASPT2(12e,12o)/cc-pVTZ-calculated energy gap between the singlet and triplet states of the CASSCF(12e,12o)/cc-pVTZ structure of **i7** (ΔE_{S-T} in (1)) is 5.1 kcal/mol.

Similar to **i1**, the channels described above leading to the two-ring species compete with direct decompositions of **i2**. Specifically, phenylallene can undergo decomposition without an exit barrier into phenyl + propargyl (**b0**), reverse to reaction R2, and H losses without reverse barriers from the CH_2 and CH groups of the side chain leading to the bimolecular products $C_6H_5CCCH_2$ + H (**b3**), -9.5 kcal/mol, and C_6H_5CHCCH + H (**b2**), reactions R4, R5, respectively. Abstraction of H from the phenyl ring the by the side chain of phenylallene (a barrier at -4.2 kcal/mol) yields the *o*-benzyne, C_6H_4 + methylacetylene, C_3H_4 product (**b6**), at -10.6 kcal/mol.

Reaction kinetics

The computed MEPs for the entrance channels of the phenyl + propargyl reaction (Figure 4) showed that the addition by the CH terminal of propargyl (R2) has a more attractive potential at R_{CC} distances below ~2.3 Å. At longer R_{CC}, the MEP potential for the addition by the CH_2 terminal (R1) is more attractive than that of CH (R2) because in this case the unpaired electron of propargyl prefers to localize on the CH_2 terminal. The dependence of the phenyl selectivity toward the two different propargyl terminals described above displays itself in the calculated temperature behavior of the VRC-TST rate constants (Figure 5) for the CH and CH_2 addition channels in the phenyl + propargyl reaction. At low temperatures, when the transition state is determined by the long-range interactions, the rate constant for the addition by the CH_2 terminal is expected to be larger than that by the CH terminal. With increasing temperature the transition states occur at shorter R_{CC} values and the attraction of phenyl to the CH terminal of propargyl grows faster than that to the CH_2 terminal. Consequently, with temperature, the rate constant for the addition by the CH terminal is expected to increase relative to that for the CH_2 terminal addition. This is indeed confirmed by the VRC-TST calculations (Figure 5). The phenyl + propargyl addition by the CH_2 terminal is characterized by the negative *T*-dependence of the VRC-TST rate constant at temperatures below 1000 K. This result is in line with the reported

previously *T*-dependence of the rate constants of the allyl + allyl,[5] allyl + propargyl,[5,18] and phenyl + allyl[7] reactions. The negative *T*-dependence in these rate constants is attributed to the bottleneck of the flux through the transition state dividing surface created by the steric repulsion of the allyl CH_2 group.[5] The present calculations showed that the phenyl + propargyl addition by the CH terminal is characterized by a positive *T*-dependence of the VRC-TST rate constant (Figure 5) indicating that in the temperature range of interest, 200 – 4000 K, the steric repulsion between phenyl and CH of propargyl does not determine the bottleneck of the flux through the transition state dividing surface. The total rate constant for the phenyl + propargyl reaction including both addition channels computed in the high-pressure-limit (HP) increases with temperature, from 5.9×10^{-11} cm^3 $molecule^{-1}$ s^{-1} at 500 K to 8.7×10^{-11} cm^3 $molecule^{-1}$ s^{-1} at 2500 K (Figure 6).

The RRKM/ME calculated *T, p*- dependent rate constants for the phenyl + propargyl reaction show a fall-off behavior above 1000, 1250, 1650 and 1800 K at pressures of 30 Torr, 1, 10, and 100 atm, respectively (Figure 6). At 2000 K, the HP rate constant for phenyl + allyl[7] is 1.2 times larger than that for phenyl + propargyl. This ratio increases with decreasing temperature, in particular, to 1.4 at 1500 K, 2.1 at 800 K, and 3.2 at 500 K (Figure 6). The *T*-dependent rate constants and relative yields computed at finite pressures of 30 Torr, 1, 10, and 100 atm for the reactions R1 and R2 are shown in Figure 7. At the typical combustion conditions (1500 K, 1 atm), the calculated rate constants for the phenyl + propargyl → 3-phenyl-1-propyne and phenyl + propargyl → phenylallene reactions are 3.2×10^{-11} and 2.8×10^{-11} cm^3 $molecule^{-1}$ s^{-1}, respectively. Below 1000 K, collisional stabilization results in the yields of 3-phenyl-1-propyne and phenylallene close to 100%, while the corresponding rate constants weakly depend on the temperature and pressure. Above 1000 K the well-skipping mechanism becomes competitive which results in a significant reactive flow into the following channels (Figure 8):

phenyl + propargyl → indenyl + H (**b1**)

phenyl + propargyl → C_6H_5CHCCH +H (**b2**)

phenyl + propargyl → $C_6H_5CCCH_2$ +H (**b3**)

At (T, p) = (1500 K, 1 atm), the calculated rate constants for the phenyl + propargyl → indenyl + H, phenyl + propargyl → C_6H_5CHCCH +H, and phenyl + propargyl → $C_6H_5CCCH_2$ +H reactions are 2.6×10^{-12}, 3.4×10^{-12}, and 3.4×10^{-13} cm^3 $molecule^{-1}$ s^{-1}, respectively. The competition between the pressure-driven collisional stabilization and temperature-driven dissociation is exhibited in the positive p-, negative T-dependences of the rate constants for the channels leading to **i1, i2** and the negative p-, and positive Arrhenius-like T-dependences of the rate constants for the channels leading to **b1-b3** (Figures 7, 8). Accordingly, the calculated branching ratios show a strong dependence on the temperature and pressure. For example, at 1500 K, 30 Torr the calculated branching ratios are 29.4% for 3-phenyl-1-propyne, 19.9% for phenylallene, 28.4% for indenyl + H, 19.6% for C_6H_5CHCCH +H, 1.7% for $C_6H_5CCCH_2$ +H, and 0.9% for indene. With increasing pressure the high-temperature product composition tends to shift back to 3-phenyl-1-propyne and phenylallene, e. g. at 1 atm the total yield of the bimolecular products **b1-b3** is 0.1%, 9.4%, 56%, and 100% at temperatures 1000 K, 1500 K, 2000K, and 2500 K, respectively, versus 0%, 1.5%, 21.5%, and 65.8% at 10 atm and the same respective temperatures. It should be noted that the direct yield of the two-ring PAH radical indenyl in the phenyl + propargyl reaction was evaluated to have a maximum of 37.2% at 1800 K and 30 Torr. The direct yield of indene via the phenyl + propargyl → indene stabilization channel was evaluated to stay below 1.4% in the combustion relevant range of temperatures and pressures, (T, p) = (500 – 2500 K, 30 Torr – 100 atm). The T, p-dependent rate constant for the phenyl + propargyl → indene reaction is given in ESI. At 1500 K, the total yield of the phenyl + propargyl products containing the two-ring PAH species indenyl and indene was evaluated at 29.3%, 5.1%, 0.9%, 0.1% at pressures of 30 Torr, 1, 10, and 100 atm, respectively. Above 2000 K, C_6H_5CHCCH +H (**b2**) becomes the major bimolecular product of the phenyl + propargyl reaction.

The phenyl + propargyl reaction can contribute to the formation of indene via secondary isomerization of collision-stabilized 3-phenyl-1-propyne and phenylallene. The T-dependent rate constants and relative yields for the isomerization/dissociations of 3-phenyl-1-propyne computed at the pressures of 30 Torr, 1, 10, 100 atm showed the following kinetically important channels:

3-phenyl-1-propyne → phenyl + propargyl (**b0**),

3-phenyl-1-propyne → indenyl + H (**b1**),

3-phenyl-1-propyne → C_6H_5CHCCH +H (**b2**),

3-phenyl-1-propyne → indene (**i4**).

The computed rate constants increase with pressure in the channels forming **i4**, **b0**, and **b2**; the opposite holds true for the channel producing **b1** (Figure 9). The rate constants for the isomerization/dissociation reactions of 3-phenyl-1-propyne show a well-defined Arrhenius behavior. At (T, p) = (1500 K, 1 atm) the computed rate constants are 3.3×10^3 s^{-1}, 2.5×10^3 s^{-1}, 9.7×10^2 s^{-1}, and 7.3×10^2 s^{-1} for the channels leading to **i4**, **b0**, **b1**,and **b2**, respectively, while at (T, p) = (2000 K, 1 atm) the corresponding rate constants are 1.3×10^5 s^{-1}, 1.2×10^6 s^{-1}, 3.4×10^5 s^{-1}, and 2.5×10^5 s^{-1}. Thus, in combustion flames, the reactions of isomerization/dissociation of 3-phenyl-1-propyne become fast enough to compete with other reaction mechanisms at 2000 K and higher temperatures. At 2000 K, the total yield of the two-ring PAH products indenyl/indene in the isomerization/dissociations of 3-phenyl-1-propyne was evaluated to be 44%, 25.1%, 18.2%, and 15.3% at the pressures of 30 Torr, 1, 10, and 100 atm, respectively, while the corresponding yield of indene is 2.8%, 6.9%, 10.6%, and 13.2%. At temperatures above 2000 K and pressures above 1 atm, phenyl + propargyl becomes the major bimolecular product of the dissociation of 3-phenyl-1-propyne.

The T-dependent rate constants and branching ratios for the isomerization/dissociations of phenylallene computed at the pressures of 30 Torr, 1, 10, 100 atm showed the following main kinetic channels:

phenylallene → phenyl + propargyl (**b0**)

phenylallene → indenyl + H (**b1**)

phenylallene → C_6H_5CHCCH +H (**b2**)

phenylallene → indene (**i4**)

phenylallene → $C_6H_5C_3H_3$ (**i5**)

The computed rate constants increase with increasing pressure for the channels producing **b0**, **b2, i4**, and **i5**, whereas, similar to 3-phenyl-1-propyne, the rate constant for the channel forming **b1** decreases (Figure 10). Again, the computed rate constants show a well-defined Arrhenius behavior (Figure 10). At (T, p) = (1500 K, 1 atm) the rate constants are 1.9×10^3 s^{-1}, 1.6×10^3 s^{-1}, 1.9×10^3 s^{-1}, 5.8×10^3 s^{-1}, and 2.4×10^3 s^{-1} for the channels leading to **b0**, **b1**, **b2**, **i4**, and **i5**, respectively; at (T, p) = (2000 K, 1 atm) the respective rate constants are 9.0×10^5 s^{-1}, 5.9×10^5 s^{-1}, 6.5×10^5 s^{-1}, and 2.8×10^5 s^{-1}. Thus, similar to the CH adduct, the direct conversion of phenylallene to the two-ring PAH species indenyl/indene is expected to become competitive only in the higher range of combustion relevant temperature, at T > 2000 K. At 2000 K, the total yield of the indenyl and indene in the channels involving the isomerization/dissociation of phenylallene was evaluated at 57.1%, 34.8%, 23.6%, and 18.5% at the pressures of 30 Torr, 1, 10, and 100 atm, respectively, while the corresponding yield of indene is 4.9%, 11%, 14.5%, and 16.1%. The yield of **b3**, $C_6H_5CCCH_2$ +H, was evaluated to stay within 4.3% when (T, p) is within the (500 – 2500 K, 30 Torr – 100 atm) range. The T, p-dependent rate constant for the phenylallene → $C_6H_5CCCH_2$ +H reaction is given in ESI. It should be noted that the $C_6H_5C_3H_3$ species (**i5**) isomerizes back to phenylallene. The T, p-dependent rate constant for the $C_6H_5C_3H_3$ → phenylallene reaction is also given in ESI.

Lastly, the kinetics calculations showed that, in the (500 – 2500 K, 30Torr – 100 atm) range of temperatures and pressures, indene dissociates mainly into the indenyl + H product, with the calculated yield of this channel being above 96% at all temperatures and pressure of interests. The T-dependent rate constant of the indene → indenyl + H reaction computed at finite pressure of 30 Torr, 1, 10, 100 atm is presented in ESI. This rate constant exhibits an Arrhenius-like T-dependence and a positive dependence on pressure. For example, at (T, p) = (1500 K, 1 atm), (2000 K, 1 atm), and (2000 K, 10 atm) the computed rate constant is 5.0×10^3, 1.7×10^6, and 3.4×10^6 s^{-1}, respectively. At temperatures above 1000 K, the computed HP rate constant for the indenyl + H recombination reaction (Figure 11) is similar to that of the cyclopentadienyl ($^2A_2$, C_{2v}) + H recombination.[36] The calculations indicate that at low temperatures, when R_{CH} in the transition state corresponds to long-range interactions, indenyl is more reactive toward H than cyclopentadienyl. Also, at low temperatures, the effect of the steric volume on the transition state

flux is exhibited by a steeper, as compared to cyclopentadienyl, negative *T*-dependence of the indenyl + H recombination rate constant.

4. CONCLUSIONS

The C_9H_8 PES related to the allyl + propargyl reaction was studied at the CCSD(T)-F12/cc-pVTZ-f12//B3LYP/6-311G** level of theory for the closed-shell singlet species and at the triplet-singlet gap CASPT2/cc-pVTZ-CCSD(T)-F12/cc-pVTZ-f12//CASSCF/cc-pVTZ level of theory for the diradical species. The state-of-the-art implementation of VRC-TST[5] was employed in the flux-through-transition surface optimizations for the barrierless channels on the computed PES. The phenomenological *T, p*-dependent rate constants were calculated using RRKM-ME.

The entrance channels of the reaction produce 3-phenyl-1-propyne and phenylallene. The reaction rate calculations showed that, at temperatures below 1000 K, collisional stabilization of the 3-phenyl-1-propyne and phenylallene adducts is the dominant reaction channel which, at high pressures, remains important up to 2500 K. As temperature grows above 1000 K, various isomerization and H elimination reactions become competitive with the collisional stabilization of 3-phenyl-1-propyne/phenylallene so that the bimolecular products C_6H_5CHCCH +H and indenyl + H become important. In particular, the computed *T, p*-dependent rate constants and relative yields of the products predict that, at pressures below 1 atm and temperatures above 1500 K, the phenyl + propargyl reaction is a significant source of indenyl + H and a minor source of indene, e. g. at 1800 K and 30 Torr the yields are 37.2% and 0.3% for the indenyl + H and indene products, respectively. Under these conditions, the calculated rate constant of the phenyl + propargyl $\rightarrow$ indenyl + H reaction is 1.35×10^{-11} cm^3 $molecule^{-1}$ s^{-1} while the rate constant for phenyl + allyl $\rightarrow$ indene is 9.77×10^{-14} cm^3 $molecule^{-1}$ s^{-1}. Thus, theoretical evidence is presented that, at combustion relevant conditions, the phenyl + propargyl recombination into the 3-phenyl-1-propyne/phenylallene adducts followed by the sequence of H shift and five-member ring closure steps via closed-shell or diradical singlet transition states is a feasible mechanism for the addition of a second five-member ring to the first six-member aromatic ring in hydrocarbon flames rich in C_3 and C_6 species. In addition, the phenyl + propargyl reaction can contribute to the formation of indenyl and indene via the secondary dissociation/isomerization of

the collision stabilized 3-phenyl-1-propyne/phenylallene. The calculations predict that, at temperatures above 2000 K, these reactions are fast enough to be of importance in kinetics of hydrocarbon flames with the total yield of indene and indenyl reaching about 20 - 50% depending on pressure.

In summary, in the combustion relevant ranges of temperature and pressure, (T, p) = (500 – 2500 K, 30 Torr – 100 atm), the following set of reactions should prove important in modeling the phenyl + propargyl association in hydrocarbon flames: phenyl + propargyl → indenyl + H, phenyl + propargyl → 3-phenyl-1-propyne, phenyl + propargyl → phenylallene, phenyl + propargyl → C_6H_5CHCCH +H, phenyl + propargyl → $C_6H_5CCCH_2$ +H; 3-phenyl-1-propyne → indene, 3-phenyl-1-propyne → phenyl + propargyl, 3-phenyl-1-propyne → indenyl + H, 3-phenyl-1-propyne → C_6H_5CHCCH +H; phenylallene → indene, phenylallene → phenyl + propargyl, phenylallene → indenyl + H, phenylallene → C_6H_5CHCCH +H; indene → indenyl + H. Modified Arrhenius expressions generated here for these reactions are collected in ESI and proposed for kinetic models.

Conflicts of interest

There are no conflicts to declare.

Acknowledgements

This work was supported by the Chemical Sciences, Geosciences and Biosciences Division, Office of Basic Energy Sciences, Office of Sciences of U.S. Department of Energy (Grant No. DE-FG02-04ER15570). We acknowledge the Instructional & Research Computing Center (IRCC, web: http://ircc.fiu.edu) at Florida International University for providing HPC computing resources that have contributed to the research results reported within this paper.

Figure captions

Figure 1. Pivot points corresponding to the active centers in the reactions a) R1, b) R2, c) R3, d) R4, f) R11 which is a substitute model of R5, g) R8, and h) R10. Reactive flux minimizations were carried out with respect to the distances shown by the dashed line.

Figure 2. Potential energy diagram for the phenyl + propargyl reaction calculated at the CCSD(T)-F12/cc-pVTZ-f12//B3LYP/6-311G** level of theory for closed-shell singlet species and radical reactants and products and at the triplet-singlet gap CASPT2/cc-pVTZ-CCSD(T)-F12/cc-pVTZ-f12//CASSCF/cc-pVTZ level of theory for diradical species. All relative energies are given in kcal/mol. Dashed lines show barrierless reactions.

Figure 3. Selected geometric parameters (bond lengths and distances in Å, angles and dihedrals in degrees) of diradical stationary structures optimized at the CASSCF(12e,12o)/cc-pVTZ and B3LYP/6-311G(d,p) (in italics) levels of theory.

Figure 4. CASSCF(12e,12o)/cc-pVDZ optimized minimal energy path with single-point energies refined at the CASPT2(12e,12o)/cc-pVDZ level for the entrance channels of the phenyl + propargyl reaction.

Figure 5. VRC-TST rate constants as functions of temperature for the entrance channels of the phenyl + propargyl reaction. Rate constants for the entrance channels of the allyl + propargyl reaction[5] are shown for comparison.

Figure 6. Temperature dependence of the total rate constant for the phenyl + propargyl reaction calculated at 30 Torr–100 atm pressures, and in the HP limit; the total HP rate constant for the phenyl + allyl reaction[7] is shown for comparison.

Figure 7. *T, p*-dependent rate constants and the relative yields for a) phenyl + propargyl $\rightarrow$ 3-phenyl-1-propyne, and b) phenyl + propargyl $\rightarrow$ phenylallene reactions. Color code: black – 30 Torr, blue – 1atm, red – 10 atm, green – 100 atm pressure.

Figure 8. *T, p*-dependent rate constants and the relative yields for a) phenyl + propargyl → indenyl + H, b) phenyl + propargyl → C_6H_5CHCCH +H, and c) phenyl + propargyl → $C_6H_5CCCH_2$ +H reactions. Color code: black – 30 Torr, blue – 1atm, red – 10 atm, green – 100 atm pressure.

Figure 9. *T ,p*-dependent rate constants and the relative yields for a) 3-phenyl-1-propyne → phenyl + propargyl, b) 3-phenyl-1-propyne → indenyl + H, c) 3-phenyl-1-propyne → C_6H_5CHCCH +H, and d) 3-phenyl-1-propyne → indene reactions. Color code: black – 30 Torr, blue – 1atm, red – 10 atm, green – 100 atm pressure.

Figure 10. *T, p*-dependent rate constants and the relative yields for a) phenylallene → phenyl + propargyl, b) phenylallene → indenyl + H, c) phenylallene → C_6H_5CHCCH +H, d) phenylallene → indene), and e) phenylallene → $C_6H_5C_3H_3$ reactions. Color code: black – 30 Torr, blue – 1atm, red – 10 atm, green – 100 atm pressure.

Figure 11. *T*-dependent HP rate constant for the indenyl + H recombination. HP rate constant for the cyclopentadienyl ($^2A_2$) + H recombination[36] is shown for comparison.

.

Figure 1

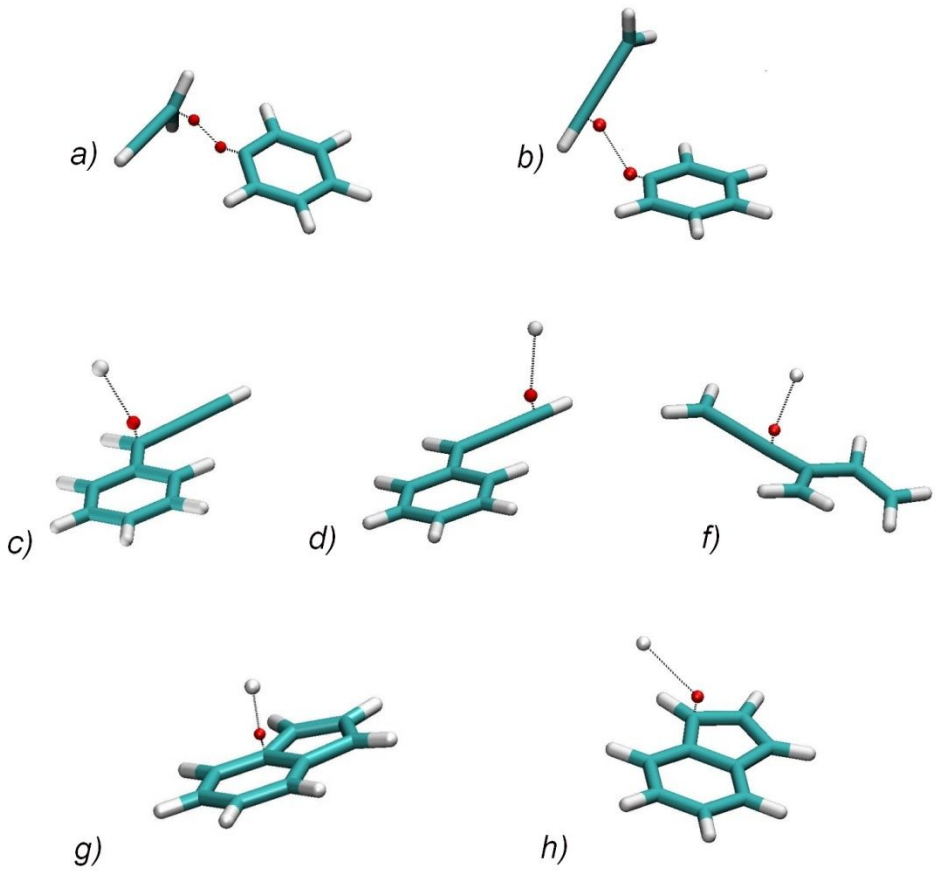

Figure 2

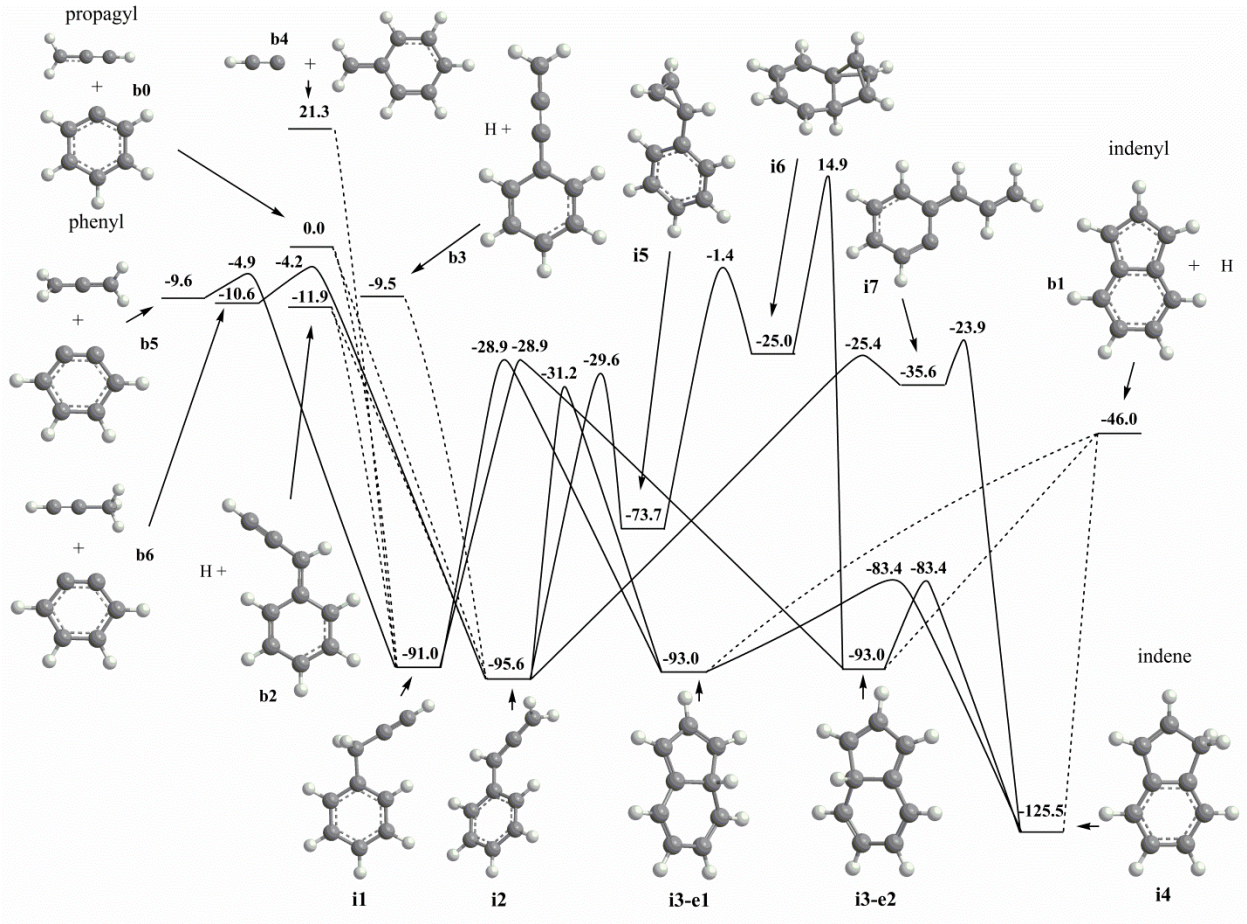
propagyl
b0
b4
21.3
H +
phenyl
0.0
b3
i5
i6
14.9
indenyl
i7
b1
+ H
-9.6
-4.9
-4.2
-10.6
-11.9
-9.5
-1.4
-25.0
b5
-28.9 -28.9
-31.2
-29.6
-25.4
-35.6
-23.9
-46.0
-73.7
b6
H +
-83.4 -83.4
-91.0
-95.6
-93.0
-93.0
indene
b2
-125.5
i1
i2
i3-e1
i3-e2
i4

Figure 3

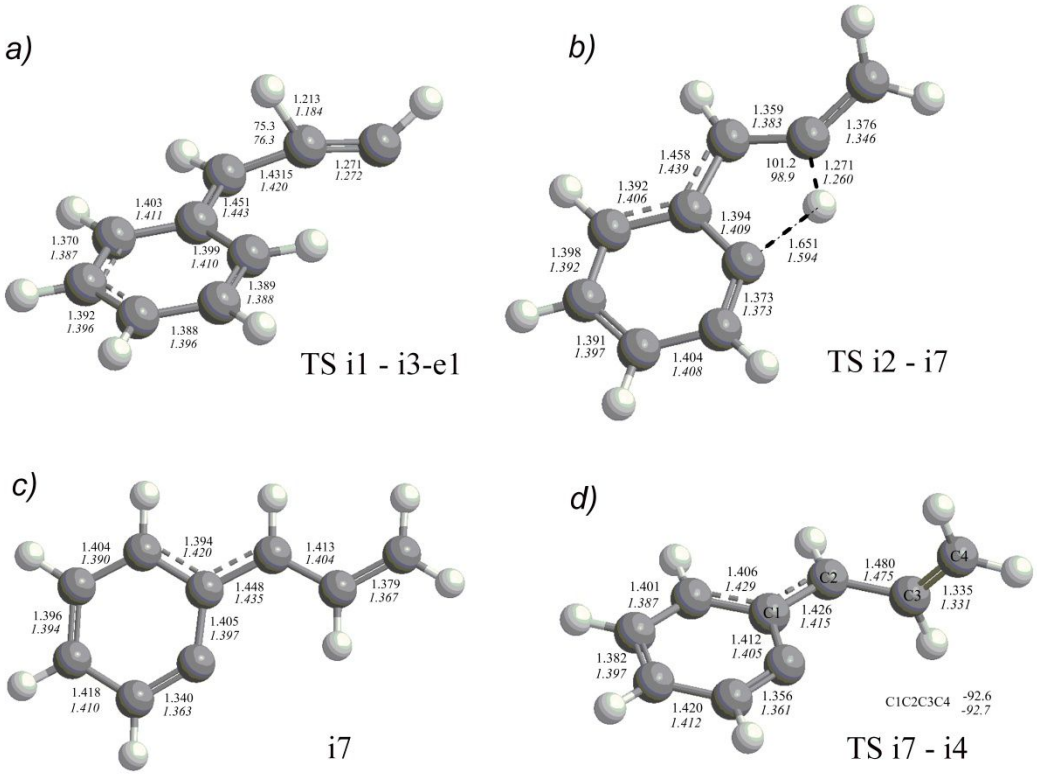
a)
1.213
1.184
75.3
76.3
1.271
1.272
1.4315
1.420
1.403
1.411
1.451
1.443
1.370
1.387
1.399
1.410
1.389
1.388
1.392
1.396
1.388
1.396
TS i1 - i3-e1
b)
1.359
1.383
1.376
1.346
1.458
1.439
101.2
98.9
1.271
1.260
1.392
1.406
1.394
1.409
1.651
1.594
1.398
1.392
1.373
1.373
1.391
1.397
1.404
1.408
TS i2 - i7
c)
1.404
1.390
1.394
1.420
1.413
1.404
1.448
1.435
1.379
1.367
1.396
1.394
1.405
1.397
1.418
1.410
1.340
1.363
i7
d)
1.406
1.429
1.480
1.475
C4
1.401
1.387
C2
C3
1.335
1.331
C1
1.426
1.415
1.412
1.405
1.382
1.397
1.356
1.361
1.420
1.412
C1C2C3C4 -92.6
-92.7
TS i7 - i4

Figure 4.

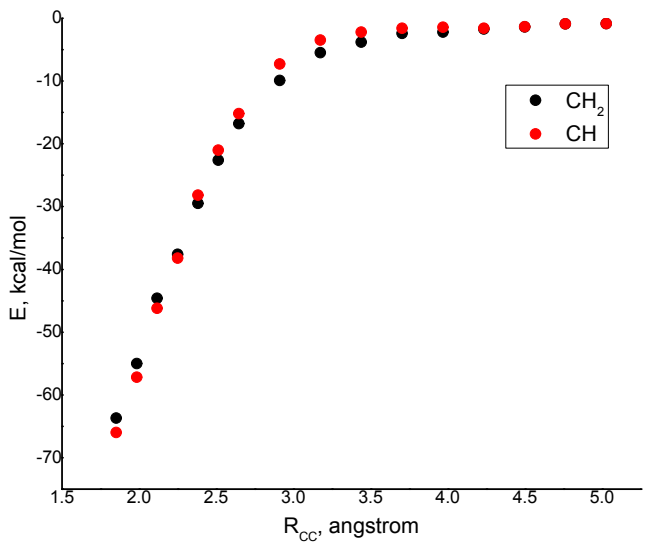
0
-10
-20
-30
-40
-50
-60
-70
E, kcal/mol
1.5
2.0
2.5
3.0
3.5
4.0
4.5
5.0
R_CC, angstrom
CH2
CH

Figure 5

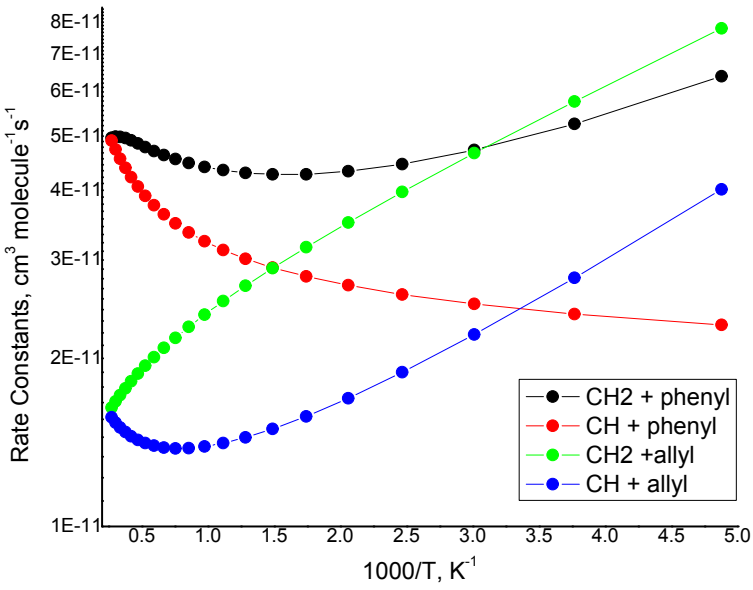
8E-11
7E-11
6E-11
5E-11
4E-11
3E-11
2E-11
1E-11
Rate Constants, cm3 molecule-1 s-1
0.5
1.0
1.5
2.0
2.5
3.0
3.5
4.0
4.5
5.0
1000/T, K-1
CH2 + phenyl
CH + phenyl
CH2 +allyl
CH + allyl

Figure 6

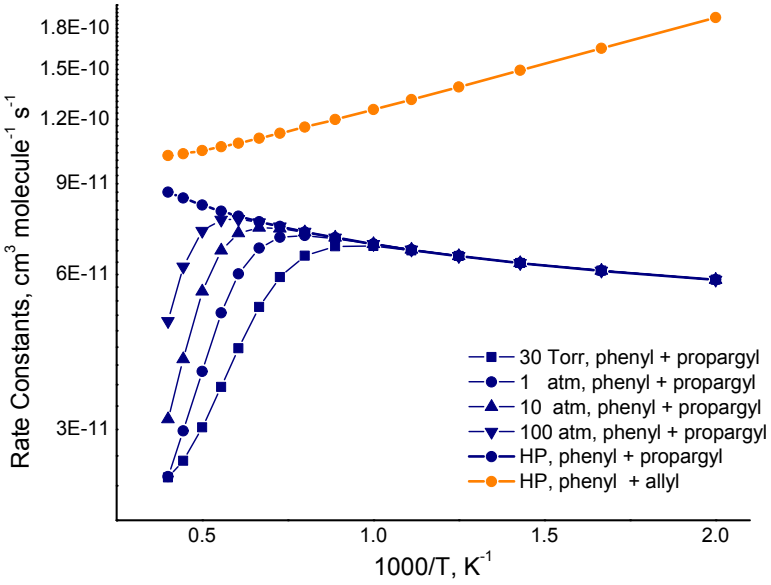
1.8E-10
1.5E-10
1.2E-10
9E-11
6E-11
3E-11
Rate Constants, cm3 molecule-1 s-1
0.5
1.0
1.5
2.0
1000/T, K-1
30 Torr, phenyl + propargyl
1 atm, phenyl + propargyl
10 atm, phenyl + propargyl
100 atm, phenyl + propargyl
HP, phenyl + propargyl
HP, phenyl + allyl

Figure 7

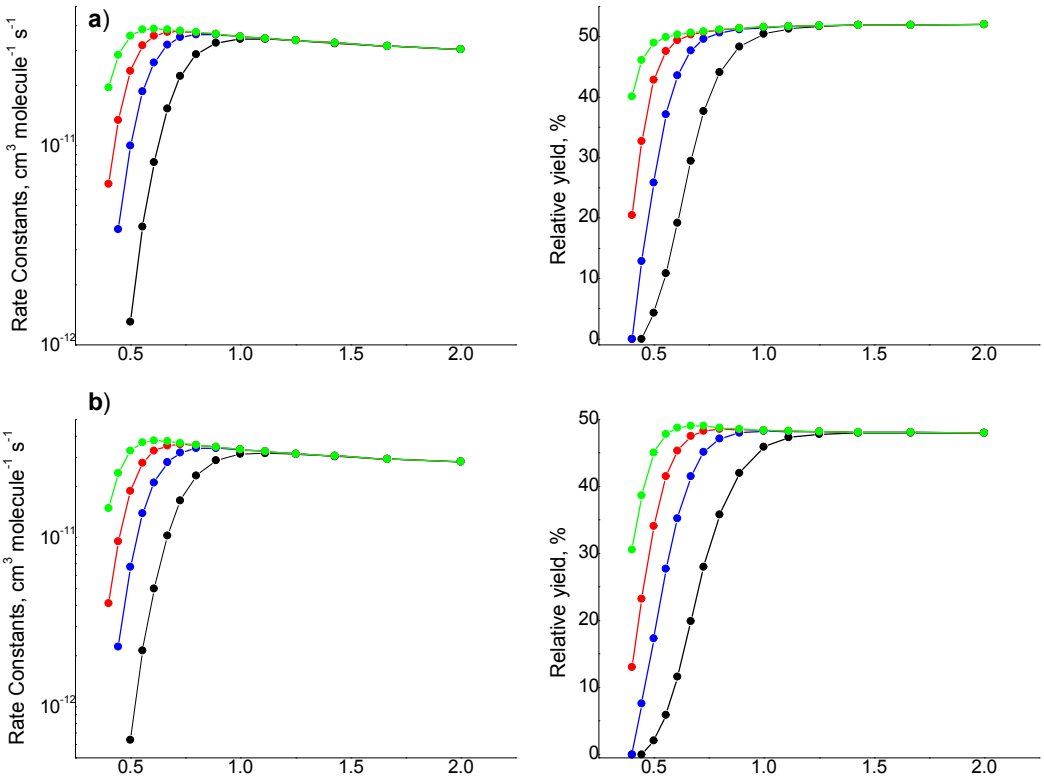
a)
b)
Rate Constants, cm3 molecule-1 s-1
Relative yield, %
10-11
10-12
0.5
1.0
1.5
2.0
0
10
20
30
40
50

Figure 8

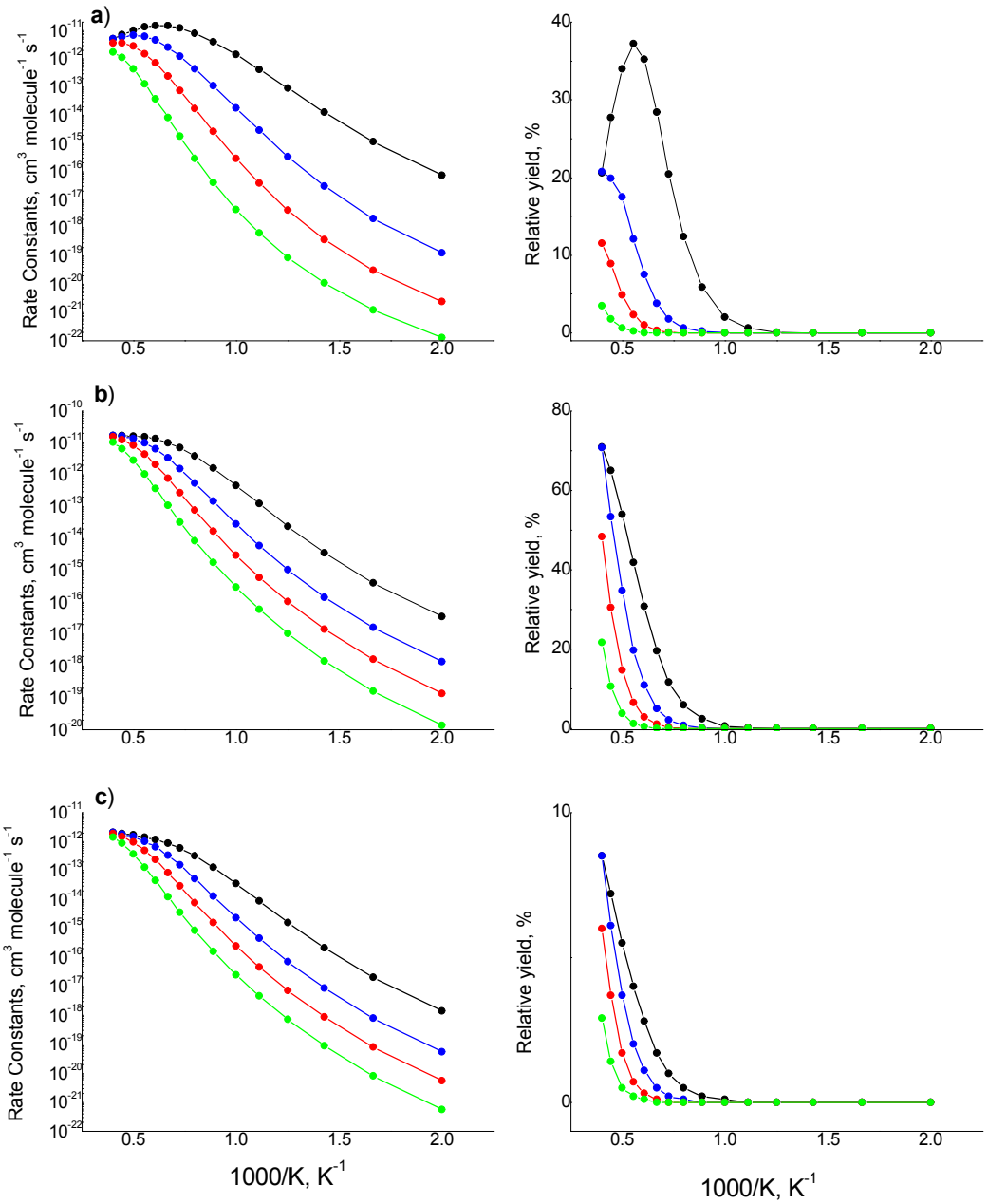
a)
b)
c)
Rate Constants, cm3 molecule-1 s-1
Relative yield, %
1000/K, K-1
0.5
1.0
1.5
2.0

Figure 9

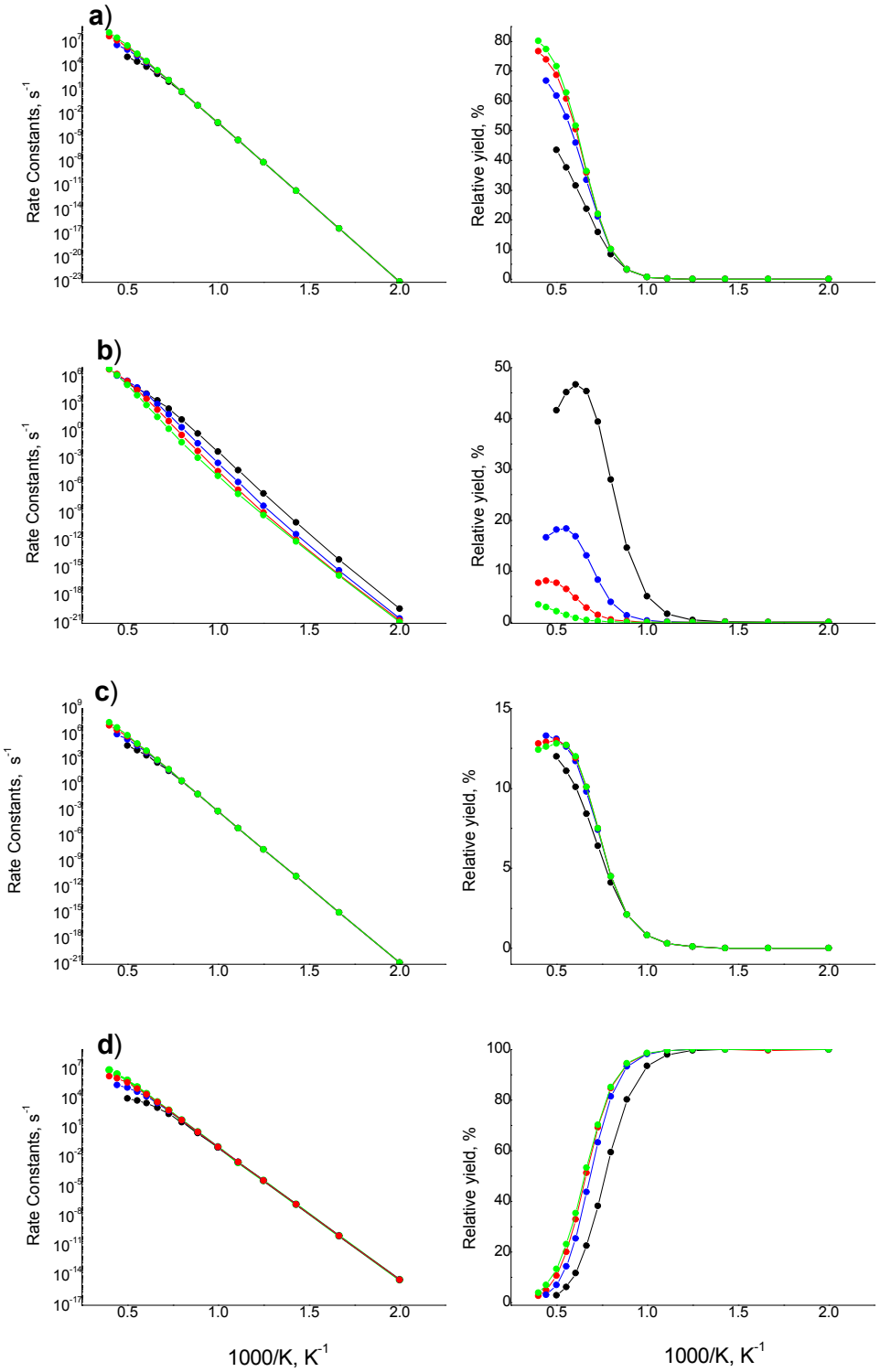

Figure 10

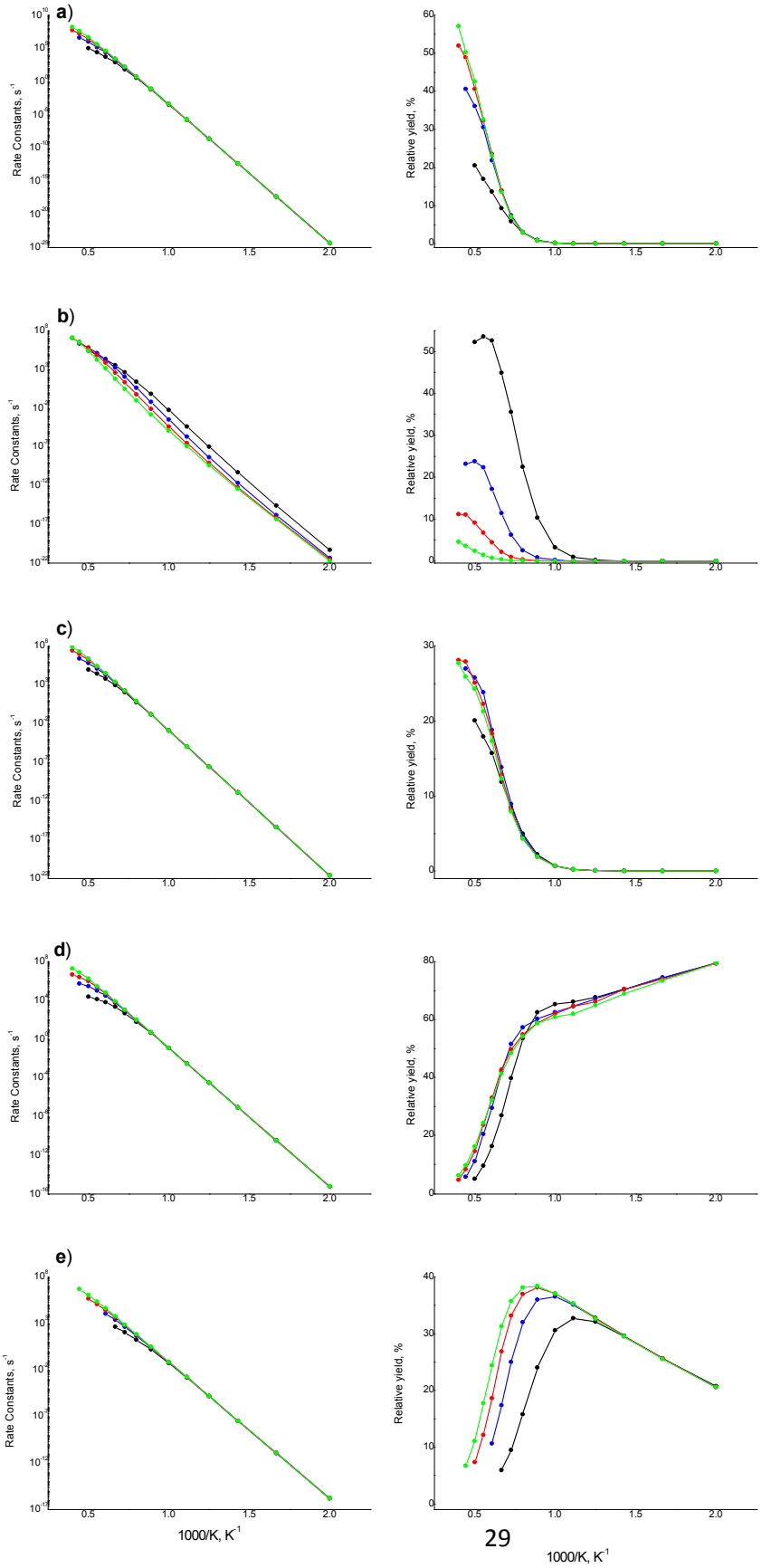

Figure 11

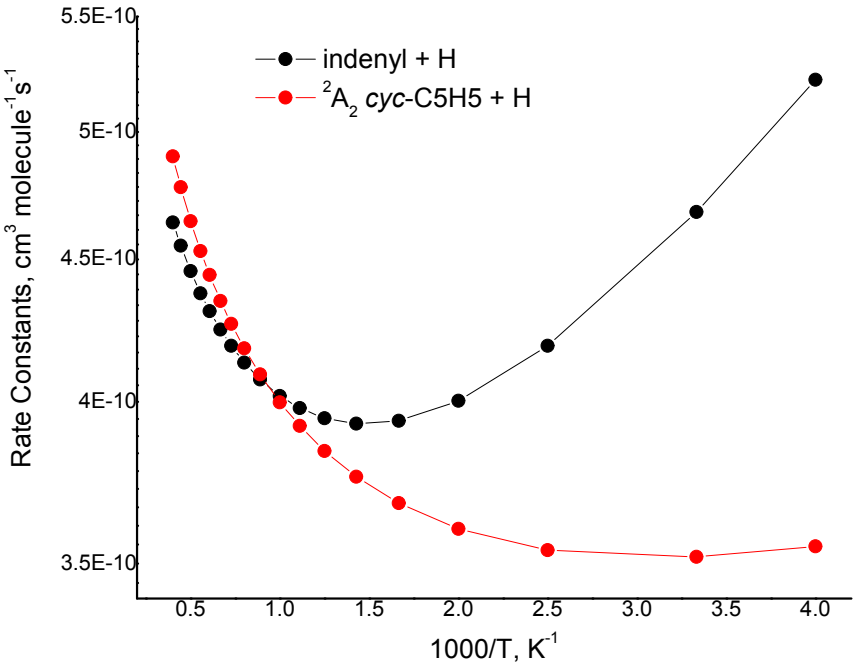
5.5E-10
5E-10
4.5E-10
4E-10
3.5E-10
Rate Constants, cm3 molecule-1 s-1
indenyl + H
2A2 cyc-C5H5 + H
0.5
1.0
1.5
2.0
2.5
3.0
3.5
4.0
1000/T, K-1

Notes and references

1 K. Kohse-Höinghaus, *Pure and Appl. Chem.*, 2019, **91**, 271-288.

2 K. O. Johansson, M. P. Head-Gordon, P. E. Schrader, K. R. Wilson and H. A. Michelsen, *Science*, 2018, **361**, 997-1000.

3 J. A. Miller, M. J. Pilling and J. Troe, *Proc. Combust. Inst.*, 2005, **30**, 43-88.

4 A. M. Mebel, Y. Georgievskii, A. W. Jasper and S. J. Klippenstein, *Faraday Discuss.*, 2016, **195**, 637-670.

5 Y. Georgievskii, J. A. Miller and S. J. Klippenstein, *Phys. Chem. Chem. Phys.*, 2007, **9**, 4259-4268.

6 A. Matsugi and A. Miyoshi, *Intern. J. Chem. Kin.*, 2011, **44**, 206-218.

7 A. N. Morozov and A. M. Mebel, *J. Phys. Chem. A*, 2019, **123**, 1720-1729.

8 L. Ruwe, K. Moshammer, N. Hansen and K. Kohse-Höinghaus, *Phys. Chem. Chem. Phys.*, 2018, **20**, 10780-10795.

9 Y. Wang, S. Park, S. M. Sarathy and S. H. Chung, *Combust. Flame*, 2018, **192**, 71-85.

10 A. W. Jasper, K. M. Pelzer, J. A. Miller, E. Kamarchik, L. B. Harding and S. J. Klippenstein, *Science*, 2014, **346**, 1212-1215.

11 V. V. Kislov, A. M. Mebel, J. Aguilera-Iparraguirre and W. H. Green, *J. Phys. Chem. A*, 2012, **116**, 4176-4191.

12 T. Dunning, H. Jr., *J. Chem. Phys.*, 1989, **90**, 1007-1023.

13 T. Adler, B., G. Knizia and H.-J. Werner, *J. Chem. Phys.*, 2007, **127**, 221106.

14 G. Knizia, T. Adler, B. and H.-J. Werner, *J. Chem. Phys.*, 2009, **130**, 054104.

15 C. T. Lee, W. T. Yang and R. G. Parr, *Phys. Rev. B*, 1988, **37**, 785-789.

16 A. D. Becke, *J. Chem. Phys.*, 1993, **98**, 5648-5652.

17 R. Krishnan, J. S. Binkley, R. Seeger and J. A. Pople, *J. Chem. Phys.*, 1980, **72**, 650-654.

18 J. A. Miller, S. J. Klippenstein, Y. Georgievskii, L. B. Harding, W. D. Allen and A. C. Simmonett, *J. Phys. Chem. A*, 2010, **114**, 4881-4890.

19 P. Celani and H.-J. Werner, *J. Chem. Phys.*, 2000, **112**, 5546-5557.

20 T. Shiozaki, G. Werner, P. Celani and H.-J. Werner, *J. Chem. Phys.*, 2011, **135**, 081106.

21 P. Siegbahn, E. M., J. Almlof, A. Heiberg and B. O. Roos, *J. Chem. Phys.*, 1981, **74**, 2384-2396.

22 H. P. Hratchian and H. B. Schlegel, *J. Chem. Phys.*, 2004, **120**, 9918-9924.

23 M. J. Frisch, G. W. Trucks, H. B. Schlegel, G. E. Scuseria, M. A. Robb, J. R. Cheeseman, G. Scalmani, V. Barone, G. A. Petersson, H. Nakatsuji, X. Li, M. Caricato, A. V. Marenich, J. Bloino, B. G. Janesko, R. Gomperts, B. Mennucci, H. P. Hratchian, J. V. Ortiz, A. F. Izmaylov, J. L. Sonnenberg, Williams, F. Ding, F. Lipparini, F. Egidi, J. Goings, B. Peng, A. Petrone, T. Henderson, D. Ranasinghe, V. G. Zakrzewski, J. Gao, N. Rega, G. Zheng, W. Liang, M. Hada, M. Ehara, K. Toyota, R. Fukuda, J. Hasegawa, M. Ishida, T. Nakajima, Y. Honda, O. Kitao, H. Nakai, T. Vreven, K. Throssell, J. A. Montgomery Jr, J. E. Peralta, F. Ogliaro, M. J. Bearpark, J. J. Heyd, E. N. Brothers, K. N. Kudin, V. N. Staroverov, T. A. Keith, R. Kobayashi, J. Normand, K. Raghavachari, A. P. Rendell, J. C. Burant, S. S. Iyengar, J. Tomasi, M. Cossi, J. M. Millam, M. Klene, C. Adamo, R. Cammi, J. W. Ochterski, R. L. Martin, K. Morokuma, O. Farkas, J. B. Foresman and D. J. Fox, Gaussian 09 Rev. A.01, Wallingford, CT, 2009.

24 H.-J. Werner, P. J. Knowles, G. Knizia, F. R. Manby and M. Schutz, *WIREs Comput. Mol. Sci.*, 2012, **2**, 242-253.

25 R. A. Marcus, *J. Chem. Phys.*, 1952, **20**, 359-364.

26 W. H. Miller, *J. Am. Chem. Soc.*, 1979, **101**, 6810-6814.

27 S. J. Klippenstein, *J. Chem. Phys.*, 1992, **96**, 367-371.

28 Y. Georgievskii and S. J. Klippenstein, *J. Chem. Phys.*, 2003, **118**, 5442-5455.

29 J. M. L. Martin and O. Uzan, *Chem. Phys. Lett.*, 1998, **282**, 16-24.

30 Y. Georgievskii, J. A. Miller, M. P. Burke and S. J. Klippenstein, *J. Phys. Chem. A*, 2013, **117**, 12146-12154.
31 Y. Georgievskii and S. J. Klippenstein, MESS Program Package, http://tcg.cse.anl.gov/papr, 2015.
32 J. Troe, *J. Chem. Phys.*, 1977, **66**, 4745-4757.
33 D. K. Malick, G. A. Petersson and J. A. Montgomery Jr, *J. Chem. Phys.*, 1998, **108**, 5704-5713.
34 Y.-Y. Chuang, J. C. Corchado and D. G. Truhlar, *J. Phys. Chem. A*, 1999, **103**, 1140-1149.
35 O. B. Gadzhiev, S. K. Ignatov, B. E. Krisyuk, A. V. Maiorov, S. Gangopadhyay and A. E. Masunov, *J. Phys. Chem. A*, 2012, **116**, 10420-10434.
36 L. B. Harding, S. J. Klippenstein and Y. Georgievskii, *J. Phys. Chem. A*, 2007, **111**, 3789-3801.

TOC Graphic